A Tumor Microenvironment-Responsive Multifunctional MoS_2-Ru Nanocatalyst with Photothermally Enhanced Chemodynamic Activity

S. Sivaselvam, R.S. Anjana, Muneer Hussain Dar, P. Kirthika and Ramapurath.S. Jayasree*

Division of Biophotonics and Imaging, Biomedical Technology Wing, Sree Chitra Tirunal Institute for Medical Sciences and Technology (SCTIMST), Trivandrum 695012, India

SI.1.1 Chemicals

Ammonium Molybdate ($(NH_4)_2MoS_4$), Thioacetamide (C_2H_5NS), 3-(4,5- dimethyl-2-thiazolyl)-2,5-diphenyl-2-H-tetrazolium bromide (MTT), Hydrogen Peroxide (H_2O_2), 2′,7′dichlorofluorescein diacetate (DCFH-DA), Dimethylsulfoxide (DMSO) and polyvinyl alcohol (PVA) were purchased from Sigma Aldrich. The cell culture chemicals and other chemical used in this work were of analytical grade and purchased from Himedia Laboratories. Ultrapure Millipore water was used in all the experiments.

SI.1.2 Characterization

Structural characteristic of the nanocomposite was analyzed using X-ray diffractometer (XRD, Ultima IV, Rigaku, Japan). The functional group of the nanocomposite was identified by Bruker Tensor 27 Fourier transform infrared spectrometer (FTIR). The EPR analysis was carried out using JEOL, JES FA200 (Japan). The EPR analysis was performed at the microwave frequency of 9.441 GHz, sweep time constant of 60s, magnetic field modulation of 100 KHz and g factor of 2.0. The morphology and elemental mapping of the prepared nanocomposite was recorded using the High-Resolution Transmission Electron Microscopy (HR-TEM, JEOL F200) operating at 200 KV. The elemental composition of the nanocomposite was determined by X-ray photoelectron spectroscopy (XPS, PHI Versaprobe III).

SI.2 Michaelis-Menton kinetics

The absorbance at 652 nm was converted to into ox-TMB generated •OH radical concentration by Beer-lambert law,

$$A=\varepsilon bc$$

Where, A is the absorbance at 652 nm, ε is the molar extinction coefficient of TMB, b is the path length and c is the concentration of ox-TMB. Then the Michaelis-Menton kinetics curve was plotted against the concentration of hydrogen peroxide *vs* initial velocity of the reaction according to the equation,

$$Vo = 1 + \frac{V_{max}\, x\, [H_2O_2]}{K_m + [H_2O_2]}$$

Where, $V_\circ$ is the initial velocity of the reaction, V_{max} is the maximum velocity of the reaction, K_M is the Michaelis-Menton constant and H_2O_2 represents the concentration of hydrogen peroxide. The value of V_{max} and K_M were obtained using the Lineweaver-Burk plot according to the following equation,

$$\frac{1}{V_0} = \frac{K_m}{V_{max}} x \frac{1}{[H_2O_2]} + \frac{1}{V_{max}}$$

SI.3 Photothermal conversion efficiency

The photothermal conversion efficiency is calculated according to previous method[1] using the formula,

$$\eta = \frac{hS\,(T_{max} - T_{surr}) - Q_{Dis}}{I\,(1 - 10^{-A\lambda})} \qquad \text{(a)}$$

Where, h is the heat transfer coefficient, S is the surface area of the container, T_{max} (55.7°C) is the maximum temperature generated in nanomaterials during laser irradiation, T_{surr} (26°C) is the ambient temperature. So, the temperature change (T_{max}-T_{surr}) in the solution of MoS_2-Ru is 29.7°C. Q_{Dis} is the dissipated heat from the solvent and quartz sample cells upon laser irradiation. I is the laser power density (1 W/cm^2) and A_λ is the absorbance of nanomaterial at 808 nm (A808 nm is 0.3).

The hS is calculated by introducing a dimensionless parameter θ as follows;

$$\theta = \frac{\square\_\ \square_{\square\square\square\square}}{T_{\square\square\square} = T_{\square\square\square\square}} \quad \text{(b)}$$

Where, T is the temperature of the solution at given time.

The *h*S is calculated using the formula, $hS = \frac{\square\square}{\tau_s}$ _____ (c)

Where, m is the mass (0.3 g), c is the specific heat density (4.2 J/g·℃) and τ_s is the slope of the cooling curve and is found to be 185. The heat dissipated from solvent and quartz sample cell (Q_{Dis}) was found to be 31.04 W. By substituting all these values in equation (a), the photothermal conversion efficiency (η) was found to be 41.01%.

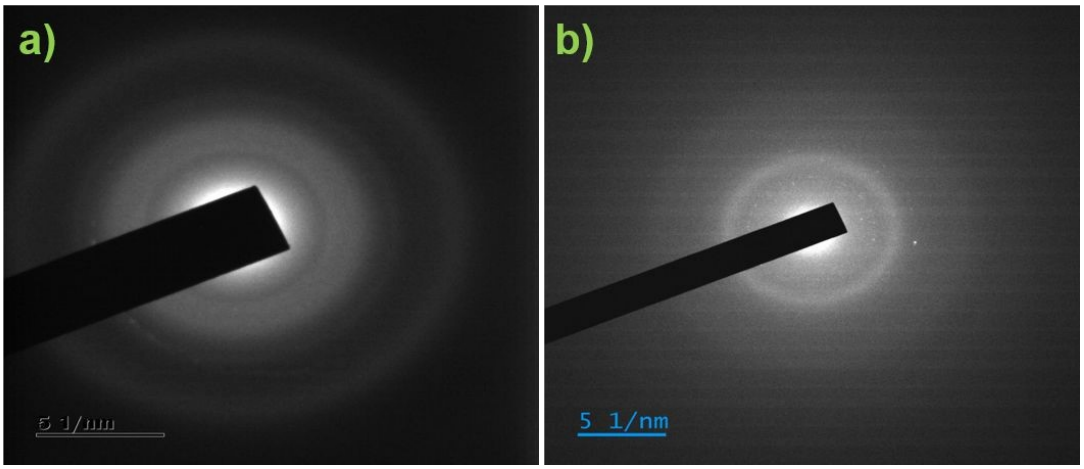

Fig. S1 SAED pattern of a) MoS_2 and b) MoS_2-Ru nanocomposite.

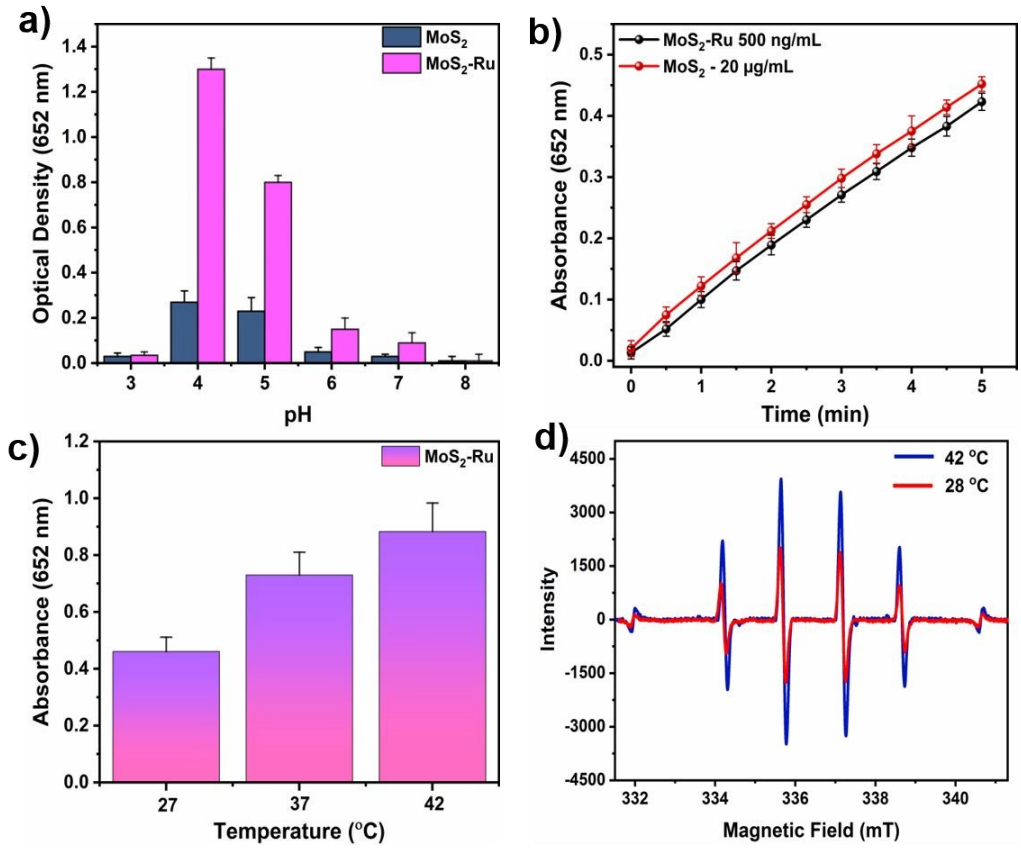

Fig. S2 a) Effect of pH on catalytic activity of MoS_2 and MoS_2-Ru. b) Comparison of time course change in absorbance of TMB under Mos_2 (20 µg/mL) and MoS_2-Ru (0.5 µg/mL). Temperature dependent hydroxyl radical production of MoS_2-Ru from c) Absorbance of TMB at 652 nm and d) EPR spectra of MoS_2-Ru at different temperature with DMPO as spin trap. Error bar represents SD of 3 experiments.

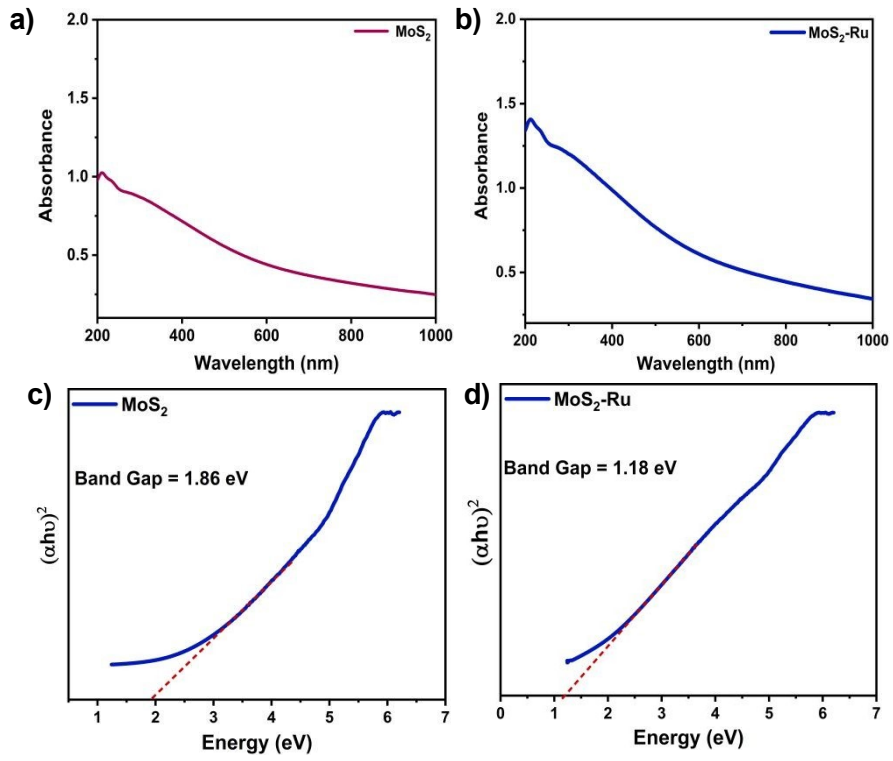

Fig. S3 Optical property of MoS_2 and MoS_2-Ru nanocomposite. UV-Visible spectra of a) MoS_2 and b) MoS_2-Ru nanocomposite. Tau plot of c) MoS_2 and d) MoS_2-Ru nanocomposite.

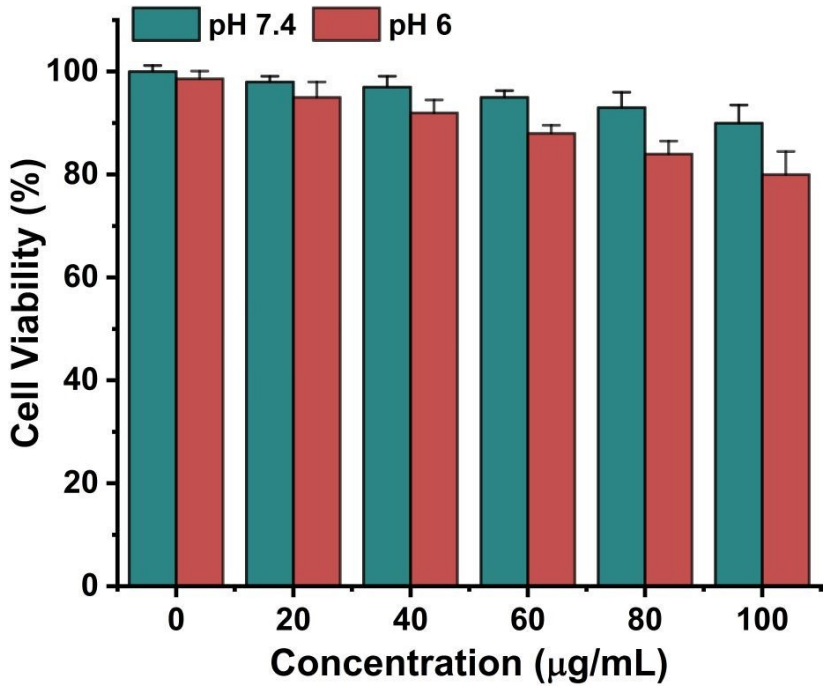

Fig. S4 Relative cell viability of MoS_2-Ru on MCF-7 cells under neural or mild acidic condition.

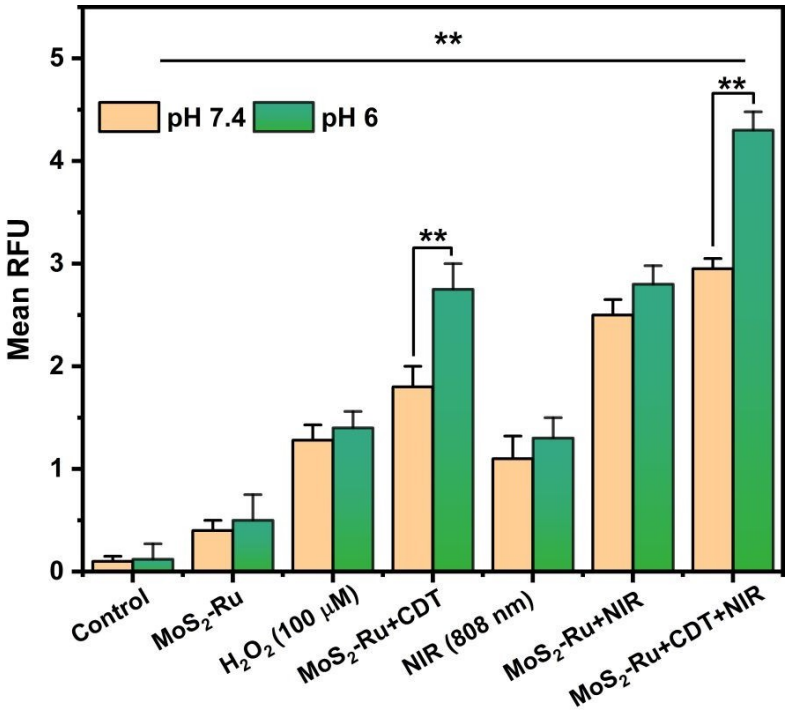

Fig. S5 Relative DCF-DA fluorescent intensity of MDA-MB-231 cells under different treatment condition. Error bar represents the SD of 3 independent experiments. ***P*<0.01.

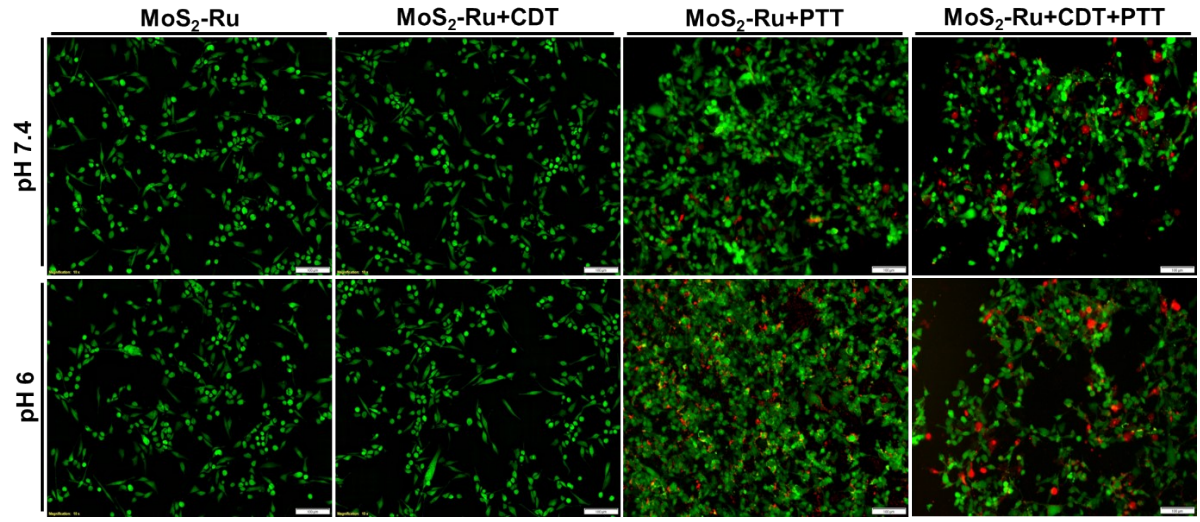

Fig. S6 Live/Dead cells in a population under different treatments.

Table S1. Comparison of photothermal conversion ability MoS_2-Ru with previous reports

S.No	Nanomaterial	Photo thermal efficiency (η)	Ref
1	MoS_2 nanosphere	37.48%	1
2	Mo@Fe-ICG nanocomposite	27.7 %	2
3	PEG-Mn nanoparticle	22.1%	3
4	FeS_2@RBC	30.2%	4
5	WO_3−x@HA	43.6 %	5
6	Cu_2-xSe	22%	6
7	Cu_9S_5 Nanocrystals	25.7 %	7
8	Mo_2C Nanosphere	24.95%	8
9	Rose Bengal conjugated GNR	21%	9
10	HPFeS_2@C-TA-PEI-GOx-FA	27.2%	10
11	Au-rGO-Fe_3O_4	19.6%	11
12	IONF@CuS	42%	12
13	MoS_2	24%	**This work**
14	MoS_2-Ru nanocomposite	41%	**This work**

References

1 J. Liu, E. Cui, Q. Zhang and D. Xie, *J Alloys Compd*, 2024, **970**, 172489.

2 B. Liu, C. Li, G. Chen, B. Liu, X. Deng, Y. Wei, J. Xia, B. Xing, P. Ma and J. Lin, *Advanced Science*, 2017, **4**, 1600540.

3 J. Ye, W. Lv, C. Li, S. Liu, X. Yang, J. Zhang, C. Wang, J. Xu, G. Jin, B. Li, Y. Fu and X. Liang, *Adv Funct Mater*, 2022, **32**, 2206157.

4 D. She, S. Peng, L. Liu, H. Huang, Y. Zheng, Y. Lu, D. Geng and B. Yin, *Chemical Engineering Journal*, 2020, **400**, 125933.

5 Y. Ding, R. Huang, L. Luo, W. Guo, C. Zhu and X. C. Shen, *Inorg Chem Front*, 2021, **8**, 636–646.

6 C. M. Hessel, V. P. Pattani, M. Rasch, M. G. Panthani, B. Koo, J. W. Tunnell and B. A. Korgel, *Nano Lett*, 2011, **11**, 2560–2566.

7 Q. Tian, F. Jiang, R. Zou, Q. Liu, Z. Chen, M. Zhu, S. Yang, J. Wang, J. Wang and J. Hu, *ACS Nano*, 2011, **5**, 9761–9771.

8 Q. Zhang, W. Huang, C. Yang, F. Wang, C. Song, Y. Gao, Y. Qiu, M. Yan, B. Yang and C. Guo, *Biomater Sci*, 2019, **7**, 2729–2739.

9 B. Wang, J. H. Wang, Q. Liu, H. Huang, M. Chen, K. Li, C. Li, X. F. Yu and P. K. Chu, *Biomaterials*, 2014, **35**, 1954–1966.

10 F. Wu, Q. Zhang, M. Zhang, B. Sun, Z. She, M. Ge, T. Lu, X. Chu, Y. Wang, J. Wang, N. Zhou and A. Li, *ACS Appl Mater Interfaces*, 2020, **12**, 10142–10155.

11 K. Jibin, M. Victor, G. Saranya, H. Santhakumar, V. Murali, K. K. Maiti and R. S. Jayasree, *ACS Appl Bio Mater*, 2021, **4**, 5742–5752.

12 A. Curcio, A. Van De Walle, E. Benassai, A. Serrano, N. Luciani, N. Menguy, B. B. Manshian, A. Sargsian, S. Soenen, A. Espinosa, A. Abou-Hassan and C. Wilhelm, *ACS Nano*, 2021, **15**, 9782–9795.

13 RV Nair, MF Puthiyaparambath, R Chatanathodi, LV Nair, RS Jayasree, *Nanoscale, 2022,* **14**, 13561-13569

14 LV Nair, Y Nagaoka, T Maekawa, D Sakthikumar, RS Jayasree, *Small*, 2014, **10**, 2771-5, 2740